

Joint stereochemical and ab initio overview of Sn^{II} electron lone pairs (E) and F⁻ (E) triplets effects on the crystal networks, the bonding and the electronic structures in a family of tin fluorides

Jean Galy^a, Samir F. Matar^{b,*},¹

^a CNRS-LCTS, Université de Bordeaux, 33600, Pessac, France

^b Lebanese German University, LGU, Sahel-Alma, P.O. Box. 206, Jounieh, Lebanon

Keywords:

Fluorides
Stereochemistry
Electron lone pair
DFT
ELF
DOS
Chemical bonding

The stereochemistry of 5s² (E) lone pair of divalent Sn (Sn^{II} designated by M*) and the lone pair triplet around the fluorine ions are examined complementarily with stereo-chemical approach and ab initio quantum investigations focusing on the electron localization and pertaining electronic structure properties, obtained within Density Functional Theory (DFT) and derived Electron Localization Function (ELF) mapping. The review completes a series of former ones focusing on the stereochemical role played by electron lone pairs LP. We start by examining LP-free Sn^{IV}F₄ then develop on Sn^{II}F₂E in its three crystal varieties (α , β , γ). The investigation then extends to study two mixed-valence fluorides: Sn^{II}Sn^{IV}F₆E₂ and Sn^{II}Sn^{IV}F₆E. The lone pair presence is readily detected in the crystalline network by its sphere of influence characterized by a radius rE, and M*-E directions; all distances are also detailed and assessed. The observations point to significant modifications of the structure which are also analyzed with the electronic density of states DOS projected over the different atomic constituents. Within the selected fluorides details of Sn^{II} various coordination numbers (CN) generally indicate one-sided coordination; specifically: CN = 4 + 1 SnF₄E triangular bipyramid, CN = 5 + 1 SnF₅E distorted octahedron (square pyramid with E roughly symmetric of its F apex) and CN = 6 octahedron [SnE]F₆. In the latter, the rotation speed of E (which increases with Z number due to relativistic effects) and the size of the F polyhedron make it favorable enough to E rotating around Sn²⁺ with the particularity of its transformation into a large cation [SnE]²⁺ with a size comparable to Ca²⁺, Sr²⁺ or Ba²⁺.

1. Introduction

The use of Tin metal (Sn) is commonly found in the canning industry for conservation and transportation for food and beverages. Chemically, upon reacting with fluorine, chlorine, sulfur, or oxygen, Sn is identified in two oxidation states: divalent Sn(II) and tetravalent Sn (IV) giving stannous and stannic compounds respectively [1]. Focusing here on Sn–F chemical combinations, stannous fluoride (SnF₂) is most known in its effectiveness against dental caries as a result of the toxicity of the various tin fluoride species that occur in solution towards bacteria which are sometimes carcinogenic. The anti-caries mechanism of SnF₂ has been investigated by determining its behavior in aqueous solution and in contact with a hydroxyl-apatite powder [2]. Further

oxidation of divalent tin fluoride leads to stannic fluoride SnF₄. From the electronic structure view, the passage from divalent to tetravalent tin is due to the loss of the 5s² electron pair LP from Sn(II) which has been shown to have large stereochemical, electronic structure, and physical effects such in enhanced ionic mobility of fluorine in PbSnF₄ [3,4]. Such LP stereo activity was also assessed in Bi(III) and Pb(II) in a review [5]. Also, mixed-valence tin fluorides with Sn(II) and Sn(IV) as Sn₃F₈ [6] and Sn₂F₆ [7] have been studied within the solid-state chemistry community to investigate the chemical effects of such mixtures which are further quantified herein.

We here provide an original assessment of tin fluorides electronic structures within coherent crystal chemistry and ab initio analyses. The investigations start from established crystal structures from the litera-

* Corresponding author.

E-mail addresses: galy@lcts.u-bordeaux.fr, jdgaly@orange.fr (J. Galy), s.matar@lgu.edu.lb, abouliess@gmail.com (S.F. Matar).

¹ Formerly at the University of Bordeaux, ICMCB-CNRS.

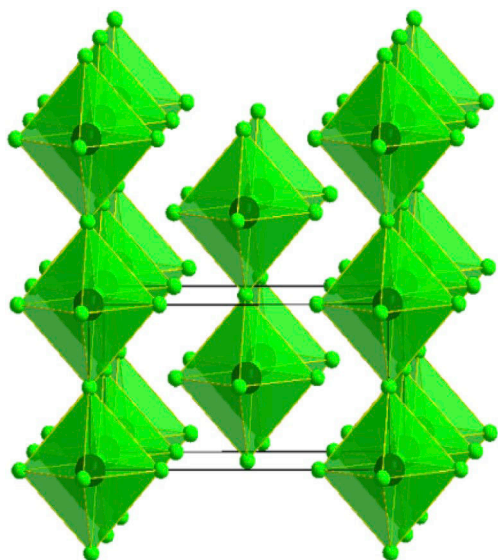


Fig. 1. Perspective view of SnF₄ tetrafluoride highlighting SnF₆ octahedra.

Table 1

X-ray and DFT-ELF (present work: pw) data of SnF₄.

SnF ₄ [22] Tetragonal, Space group I4/mmm (N°139) Molecular weight: 194.684g, ρ _x = 4.88 (g/cm ³)						
	a (Å)	b (Å)	c (Å)	V (Å ³)	Z	rV(F,E) (Å ³)
RX [21]	4.0498	4.0498	7.9375	130.18	2	16.3
DFT-ELF [pw]	4.05	4.05	7.94	130.20	2	16.3
Interatomic distances (Å) and angles (°) – DFT – ELF analyses - [*] average						
Sn-F1 eq	2.025	F1-F1	2.864	Sn-CT	2.042	
Sn-F2 ax	1.874	F2-F1	2.759			
E2-F2	0.560	E2-CT	0.534	Sn-E2 (of {F2E2 ₃ })	0.560	
T. rd.rect.F2	2.13/	∅Text.{F2E2 ₃ }	1.94	Tgyr. yellow circle - radius	0.534	
Fig. 3 L/H/R	1.50/0.65	blue dotted circle				
E2 ellipsoid a/b/c	0.49/0.49/0.76	rE2 Sphere of influence.	0.57	CT-F2	0.168	

[pw]: present work.

eq.: equatorial. ax.: axial. Ec2 coordinates: x,y,z (Wy (32o) site), 0.9631/0.5135/0.7572.

CT: E2 torus center Wyckoff positions: Wy x,y,z 0.5/0.5/0.7573. T gyr. E2: torus gyration radius = 0.534 Å.

ture, followed by calculations based on the quantum density functional theory (DFT) [8,9] targeting data pertaining to the electron localization description based on the electron localization function (ELF) approach by Becke and Edgecomb [10]. As a matter of fact, we have shown in former works [3, 5 and therein cited refs.] that the stereochemistry and metrics of electron lone pairs (LP) can be accurately addressed from merging together quantum chemical calculations within DFT and crystal chemistry rationale.

The purpose of this work is to apply this methodology to examine Sn LP in the three experimental varieties of SnF₂ α, β and γ [11,12] and the above-mentioned mixed-valence fluorides. For the sake of

completeness, the electronic structures are addressed based on the site projected electronic density of states DOS; we also provide a qualitative description of chemical bonding based on the overlap populations.

2. Brief description of the computation methodology

Within DFT we used VASP (Vienna ab initio simulation package) code [13,14]. The projector augmented wave (PAW) method [14,15], was used with atomic potentials built within the generalized gradient approximation (GGA) scheme [16].

A major outcome from electronic structure calculations is the electronic charge density and the electron localizations which are addressed based on their localization function ELF [10]. ELF is a scheme firstly devised for Hartree-Fock quantum chemical calculations. Later on, its extension to DFT methods was done by Savin et al. [17] as based on the kinetic energy with explicit account for the Pauli Exclusion Principle: $ELF = (1 + \chi_{\sigma}^2)^{-1}$. In this expression the ratio $\chi_{\sigma} = D_{\sigma}/D_{\sigma}^0$, where $D_{\sigma} = \tau_{\sigma}^{-1/4} (\nabla\rho_{\sigma})^2/\rho_{\sigma}$ and $D_{\sigma}^0 = 3/5 (6\pi^2)^{2/3} \rho_{\sigma}^{5/3}$ correspond respectively to a measure of Pauli repulsion (D_{σ}) of the actual system and to the free electron gas repulsion (D_{σ}^0) and τ_{σ} is the kinetic energy density; ρ being the electron density. A normalization of the ELF function between 0 (zero localization) and 1 (strong localization) with the value of 1/2 corresponding to a free electron gas behavior enables analyzing the 2D contour maps following a code: blue zones for zero localization, red zones for full localization and green zone for $ELF = 1/2$. Besides the 2D ELF representation, we mainly consider the metrics of 3D iso-surfaces enclosing the electrons of LP atomic constituents. We note here that regarding electron localization another choice is to use Wannier localized functions in real space (like ELF) for a chemical insight [18].

Site projected density of states PDOS analyses were carried out using scalar relativistic full potential augmented spherical wave ASW method (for more details cf [19,20]. and cited refs therein). Also when pertinent for further argumentation, the chemical bonding is addressed following Hoffmann with the COOP criterion (crystal orbital overlap population) based on the overlap integral S_{ij} ; i and j being two chemical species, ex. Sn and F [21].

3. Tin (IV) fluoride: SnF₄

3.1. Description and crystal chemistry rationale

There is only one tin fluoride phase with a maximum IV oxidation state, SnF₄; it is a hygroscopic white powder. In its crystal structure, the fourfold axes of the SnF₆ octahedra are parallel to [001] and corner-shared via their entire equatorial apices parallel to (001) plane. They form [SnF₄]_n monolayers parallel to this plane. These layers are packed along [001] with c/2 periodicity and a shift of $1/2\vec{a} + 1/2\vec{b}$ (Fig. 1). The relevant X-ray data from Bork and Hoppe [22] are reported in Table 1 and the perspective view of the structure highlighting the SnF₆ octahedra is represented in Fig. 1.

The SnF₆ octahedra, opposite to regular SnO₆ ones are flattened with shorter apical bonds Sn-F2 (x2) = 1.874 Å versus longer equatorial ones Sn-F1 (x4) = 2.025 Å. The fluorine equatorial plane is perfectly tetragonal with (4x) F1-F1 = 2.864 Å, the remaining apical-equatorial bonds being smaller (8x) F-F = 2.759 Å. It is relevant to note that both Sn atoms and F2 sit onto fourfold rotation axis with Wy 2a 4/mmm (0,0,0) for the former and Wy 4e 4mm for the second (Wy = Wyckoff position).

These pieces of data are significant upon assessing the evolution of cell volumes and interatomic distances when fluorides of crystal Tin II structures are considered and particularly the role played by the 5s² lone pair of Sn(II) and also by {2s²2p⁴} configuration of 3 LP's (triplets)

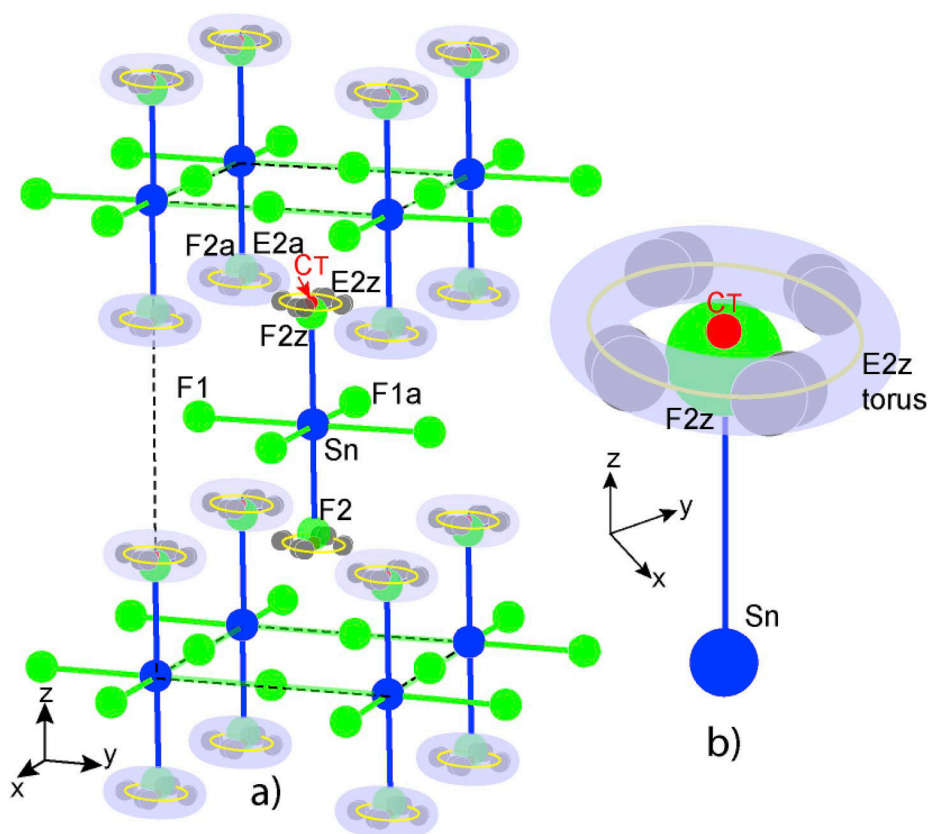


Fig. 2. SnF_4 a) Perspective view of the packing of monolayers $[\text{SnF}_4\{\text{E}_3\}_2]_n$; b) Detail of the most important piece of the network the $\text{Sn-F}_2\{\text{E}_3\}$ with the electronic torus (pale blue) generated by fluorine $2s^2 2p^4$ lone pair triplet whirling around Sn-F_2 direction at CT level at 0.168 \AA from F_2 ($\text{Sn-CT} > \text{Sn-F}_2$) (CT: indicates E2 torus center). (For interpretation of the references to color in this figure legend, the reader is referred to the Web version of this article.)

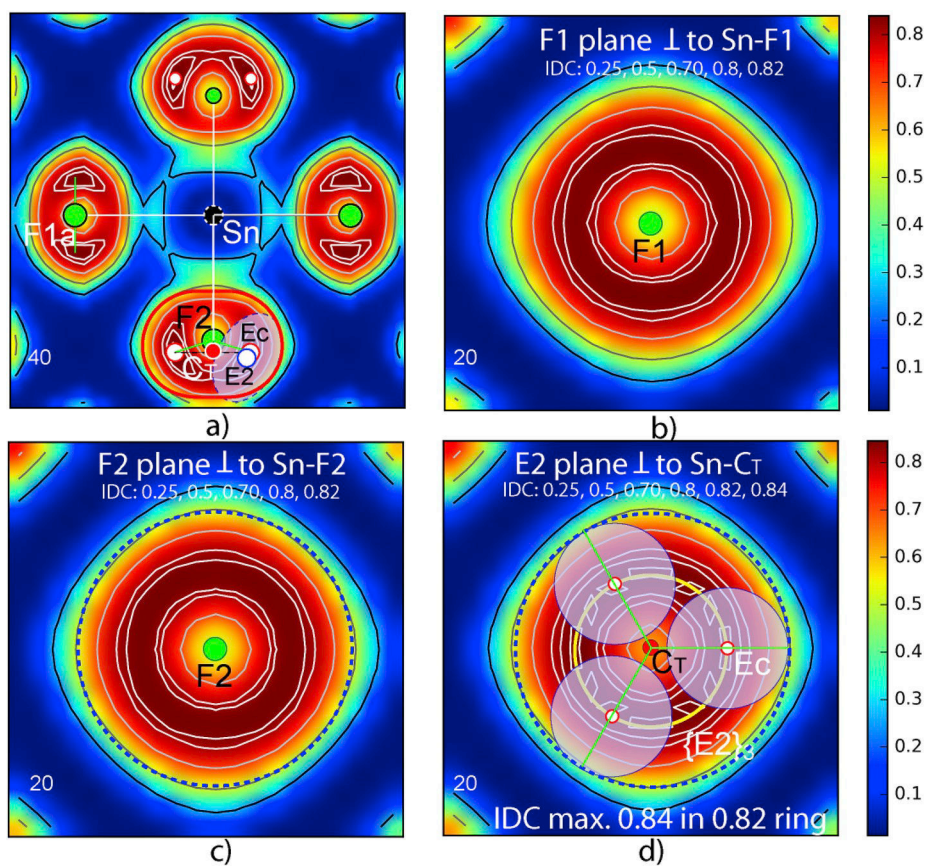


Fig. 3. SnF_4 a) ELF section by (SnF_1F_2) plane which is parallel to $[001]$ with A_4 fourfold rotation axis coiling to Sn-F_2 bond. Note the symmetric high densities below F_2 where E_2 whirling around leaves its trace (CT middle of the symmetric Ec-Ec); Ec white-red circle exact position and circle white-blue E_2 the center of ellipse section of the electronic cloud accompanying Ec . b) Planar section perpendicular to Sn-F_1 in F_1 ; note the regular electronic ring with $\text{IDC} = 0.84$. c) The same type of section but perpendicular to Sn-F_2 in F_2 ; note the large ring with the highest $\text{IDC} = 0.82$. d) The section passing by CT remarkably different with, in the domain of the ring with $\text{IDC} = 0.82$, eight domains with $\text{IDC} = 0.84$ these domains perfectly described by tetragonal space group $I4/mmm$ and designed by dark-grey circles in Fig. 2b. E's then move continuously along the gyration circle (yellow trace).

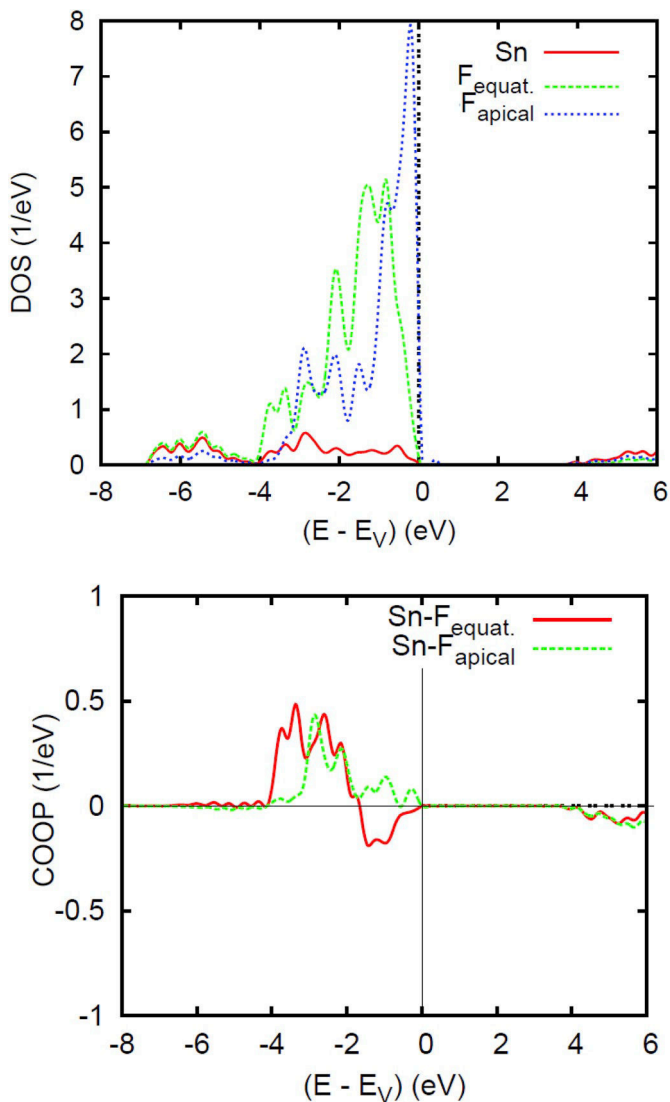


Fig. 4. SnF_4 : Site projected DOS (top) and chemical bonding using COOP criterion (bottom) based on the overlap integrals.

Table 2

Crystallographic [11] and DFT -ELF [pw] data of α SnF_2E .

α SnF_2 - [11] Monoclinic - Space group C2/c (N ¹⁵) - Molecular weight: 156.686 - $\rho_x = 4.88$ (g/cm ³).							
	a (Å)	b (Å)	c (Å)	β (°)	V (Å ³)	Z	rV(F,E) (Å ³)
Crystal [11]	13.3532	4.9073	13.7860	109.29	852.66	16	17.8
DFT-ELF [pw]	13.3532	4.910	13.786	109.30	854.40	16	17.8
Interatomic distances (Å) & angles (°) - 1) crystal - 2) ELF analyses							
1)	Sn1-F2 eq	2.102	Sn2-F1ap	2.048	\angle F2Sn1F3c eq	86.7	
	Sn1-F3c eq	2.057	Sn2-F1	2.386	\angle F3iSn1F4a ax	142.7	
	Sn1-F4a ax	2.156	Sn2-F2	2.197	\angle Sn1F2Sn2	172.0	
	Sn1-F3i ax	2.671	Sn2-F4	2.276	\angle Sn2F4Sn1a	131.3	
	F1ap- F1	2.890	Sn2-F3	2.494	F3i-F3c	2.737	
2)	Sn1-E1	0.86	Sn2-E2	0.99	\angle E2Sn2F1ap	175.2	
	E1-F2 eq	2.45	E2-F1	2.70			
	E1-F3c eq	2.90	E2-F2	2.60			
	E1-F4a ax	2.55	E2-F3	2.83			
	E1-F3i ax	3.00	E2-F4	2.69			
	E1a-E2	2.55	E2-E2a	2.91			
	E1 ellipsoid a/b/c	1.27/1.14/0.80	E2 ellipsoid a/b/c	1.30/1.10/0.84	rE1	1.05	
					rE2	1.06	

eq: equatorial; ax: axial. Ec coordinates: 0.1205/0.1476/0.4145 (Ec1); 0.0624/0.3442/0.1814(Ec2).

E a/b/c ellipsoid size - rE: radius of the sphere of influence.

rV(F,E): reduced volume = cell volume divided by number of F + E.

which are all non-bonding in "apical" fluorine atoms.

Therefore while examining Sn fluorides it is important to focus also on the stereochemistry and the topology of F^- electron pair triplets derived from ab initio calculations. For this purpose performing calculations of the electronic structure within DFT and deriving the Electronic Localization Function (ELF) on fluorine lone pair triplet within SnF_4 were carried out and their experimental [22] and calculated data are listed in Table 1.

In SnF_4 network there is an important feature concerning the monolayers, F1 the equatorial atom, in between two Sn atoms design a planar two-dimensional network while F2 strongly connected to Sn ($\text{Sn-F2} = 1.874$ Å) points apart this plane. This is shown in Fig. 2a and b.

Two F2 levels (F2z and F2a) pertaining to two successive SnF_4 layers do not interpenetrate and show a thin interspace of 0.221 Å (F2z ($z = 0.7361$) and F2a ($z = 0.7639$) left to F-F interactions.

Therefore it was important to localize precisely the lone pair triplet $\{E_3\}$ potentially associated with F2 atoms to understand the $[\text{SnF}_4]_n$ layer packing. Note that we have shown the stereochemical importance of $\{E_3\}$ triplets whirling around their atom in preceding compounds like XeF_2E_3 [23], OF_2E_8 or Cl-FE_3 [24] as revealed by similar DFT-ELF calculations.

3.2. Electron localization function ELF

The $\{E_3\}$ triplets around F2z were derived and refined from ELF data. So in a first attempt, a search of a maximum E2z density around F2z in the three-dimensional electron localization was done and E2z coordinates determined and refined. These coordinates correspond to the general position Wyckoff position Wy 32 o x,y,z (see Table 1). Fig. 3a shows a section of SnF_4 layer by a plane SnF1F2 ; it gives information of paramount importance concerning the two independent crystallographic sites of F atoms. F1 assuming a connection of Sn atoms in a square net shows an ellipsoid well centered on it, and confirmed by a section in Fig. 3b where a regular ring of iso-density curve $\text{IDC} = 0.84$ is centered on F1 ($\text{IDC} = \text{isodensity curve}$). Then F2 appears immediately more complex in Fig. 3a with two symmetric maxima (white-red) circles showing a line perpendicular to Sn-F2 but clearly non-centered on F2 but in CT onto the fourfold axis.

After space group symmetry operations the triplet of lone pairs around F2z $\{E2z\}_3$ shows eight equivalent positions (marked by dark grey circles - see Fig. 2a) around the fourfold rotation axis, forming a

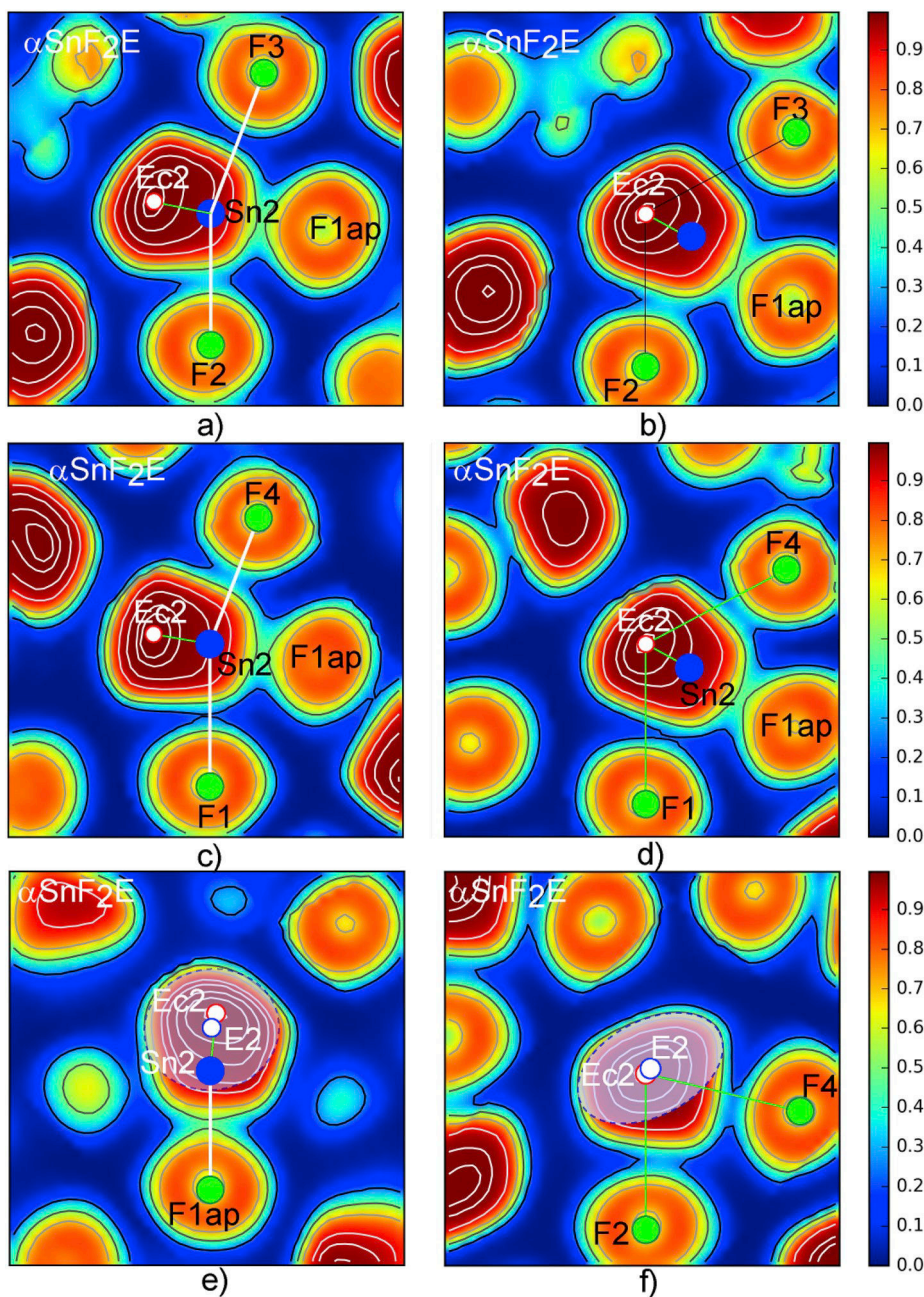


Fig. 7. α SnF₂. a), b), c), d) ELF sections depicting planes with diagonal F2F3 and F1F4 of the fluorine square pyramid with Sn2 and E2. e) plane containing the Ec2-Sn2-F1ap the pseudo fourfold axis of the Sn2F₅E2 octahedron, also showing one section of E2 (pale blue ellipse). f) A planar section Ec2F2F4 showing another section of E2 giving a second parameter set of lone pair ellipse (pale blue). (For interpretation of the references to color in this figure legend, the reader is referred to the Web version of this article.)

circle which center CT on fourfold axis shows E2z coordinates clearly of center from F2z further from Sn (CT-F2 = 0.168 Å, Sn-CT > Sn-F2z by 0.221 Å). So important to note that if the layers [SnF₄]_n along [001], bordered by F2 do not interpenetrate, leaving an “empty” two-dimensional space, in fact, this space is filled up by two E2 layers, E2z and E2a, therefore with a sequence F2z/E2a/E2z/F2a and $\Delta(F2z-E2a) = 0.052$ Å, $\Delta(E2a-E2z) = 0.116$ Å and $\Delta(E2z-F2a) = 0.052$ Å. The {E₃} triplet, in principle, cannot accept a fourfold axis, so, the best solution is to consider that the three doublets are whirling around it

(drawn as a torus including all the eight dark-grey circles (Fig. 2a and b)). Now the {SnF₄{E₃}₂}_n layers are held together by these E2z and E2a which interpenetrate. This association cannot be very strong and it is not surprising to note its high hygroscopicity which makes it difficult to handle, but in return its high reactivity can be directly reliable to these (001) planes whose surface presents very active whirling electron doublets being capable to play as chemical scissors in contact with another material.

Fig. 2b shows the detail of Sn-F2{E₃} bonding. E lone pair

Table 3
X-ray and DFT-ELF data of β SnF₂E.

β SnF ₂ E - [11] Orthorhombic - Space group P2 ₁ 2 ₁ 2 ₁ (N°19) - Phase transition 339K. Molecular weight: 156.686 - $\rho_x = 5.25(\text{g}/\text{cm}^3)$.						
	a (Å)	b (Å)	c (Å)	V (Å ³)	Z	rV(F,E) (Å ³)
RX [3]	4.9889	5.1392	8.4777	217.36	4	18.1
DFT-ELF	4.8030	5.1300	8.0460	198.25	4	16.5
Interatomic distances (Å) & angles (°) - DFT - ELF analyses - * average						
Sn-F1 ap	2.131	Sn-F2	2.358	Sn-F*eq	2.379*	
Sn-F1a	2.336	Sn-F2c	2.668	F1ap-F*	2.888*	
Sn-F2b	2.153	F1a-F2b	3.122	\angle F1apSnF*	79.5*	
F2b-F2	2.862	F2-F2c	3.868	\angle ESnF*	101.1*	
F2cF1a	3.386	F1-F1a	2.823	\angle ESnF1ap	162.7	
Sn-E	1.019	Ec ... Eb	2.941	E-F*	2.756*	
E ellipsoid a/b/c	1.13/1.07/1.00			rE	1.07	

Eq.: quadrilateral equatorial. F* equatorial for averages.

Ec coordinates: 0.9643/0.3917/0.3368.

E a/b/c ellipsoid size - rE: the sphere of influence.

dimension has been evaluated with its center dark-grey surrounded by an electronic cloud in form of an ellipsoid (pale blue ellipse, a/b/c parameters derived from Fig. 3a,c,d). It is reasonable to postulate that the three E's would be separated by 120°. In Fig. 3d the ring of IDC = 0.82 E's leaves eight preferential spots of various sizes with IDC = 0.84 during their whirling around Sn-CT axis. {E₃} triplet is set into a torus whose size and gyration circle have been precisely delimited. In the torus E's are reasonably separated by 120°; three green radii (green sticks) being drawn to note that during the jumps of E from one large density "island" to another the three sticks are roughly

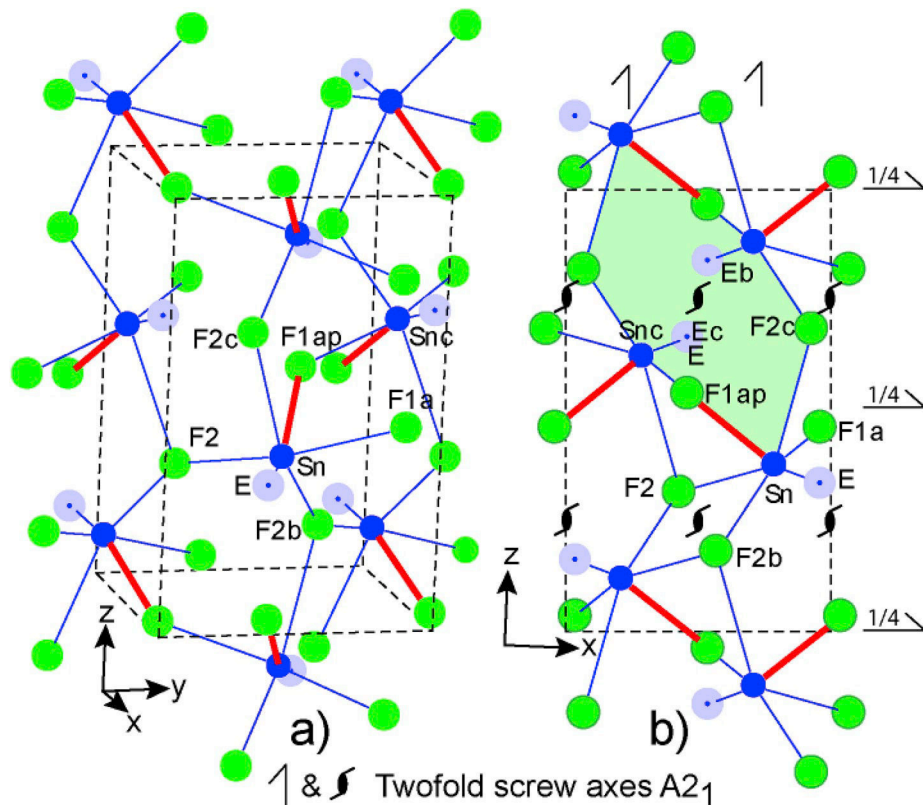


Fig. 8. a) The β SnF₂ three-dimensional network built up by [SnF₅E] octahedra sharing apices but the E one; the apical bonds Sn-F1ap opposite to Sn-E are shown by red sticks. b) A projection onto (010) plane allows to enlighten the tetramer [Sn₄F₄] shaded in pale green and the presence of two Sn-F1ap over the eight Sn-F surrounding it; worthy to note that the green tetramer [Sn₄F₄] is centered around a twofold screw axis developing a channel welcoming two lone pairs sites (E and Ec). (For interpretation of the references to color in this figure legend, the reader is referred to the Web version of this article.)

continuously pointed onto a domain of maximum density IDC = 0.84. So the whirling around A4 axis of E's is self-propelling to overcome a potential little difference when {E₃} doublets jump from one IDC domain to another (at the vicinity of 45° the symmetric domains with IDC = 0.84 are reduced).

3.3. Electronic density of states and chemical bond

The upper panel of Fig. 4 shows the site-resolved projected DOS (density of states) PDOS projected on Sn and the two fluorine sites F_{eq} (F1) and F_{ap} (F2z). In this plot and all the following ones, the zero of energy is with respect to the top of the valence band (VB) at E_V. This is why VB energies are negative whereas those of the empty conduction band (CB) are positive. The energy gap between VB and CB amounts to 4 eV. Then the tetrafluoride can be qualified as a wide gap insulator. The DOS in the VB spans two regions from -7 to -4 eV for low energy lying s-like states and from -4 eV up to E_V for p-like states. In the former region, there can be seen quite similar Sn and F-eq (F1) PDOS skylines, which are different from those of F_{ap} showing lower magnitude. This is also observed for the p-like states for the Sn-F_{eq} (F1) albeit with much larger intensity for F states especially for F_{ap} (F2z) which show the largest intensity especially at the top of VB.

The lower panel shows the comparative bonding between Sn and the two F sites. The Sn-F2z (equatorial fluorine) bonding is clearly stronger especially around -4 eV in spite of negative antibonding COOP between -2 and the top of VB. Oppositely Sn-F_{ap}. COOPs are lower in intensity but keep bonding (positive COOP) up to VB-top. This highlights the nonbinding character of the intense states of F_{ap}, which are actually responsible for the development of tori around F as shown in Fig. 2.

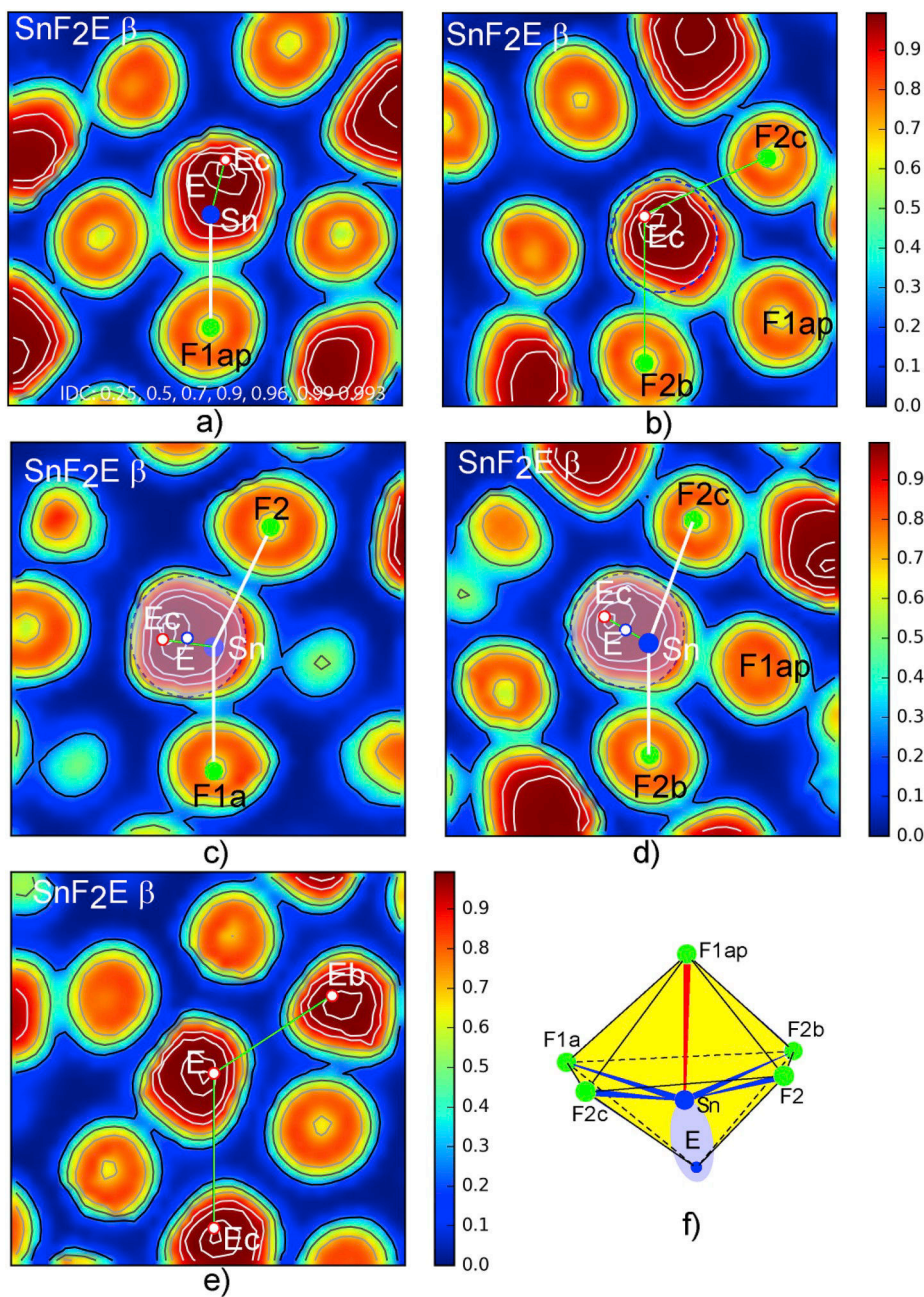


Fig. 9. β SnF₂. a) ELF data section by F1ap-Sn-Ec plane underlines E position on the line of F1ap-Sn apical bond. b) EcF2bF2c and the presence F1ap trace are roughly in the same plane. c) & d). These sections show that Sn-F1a, F2, F2b bonds are linked by the continuity of electron density while Sn-Fc clearly longer is attracted by two Sn atoms (Fig. 9d). e) A section in the double endless chain of E in the tetramer channel depicted in Fig. 9b f) The typical one-sided CN = 5 + 1 of tin in the form of distorted octahedron SnF₅E with Sn(II) and its E being opposite to F1ap.

4. Tin (II) fluorides

4.1. α SnF₂

Focusing firstly on the base centered monoclinic difluoride α SnF₂, the structure shows all atoms at (8f) Wyckoff positions with two different Sn and four F. Cell data are reported in Table 2; same atomic coordinates for all atoms in both X-ray and DFT-ELF data.

α SnF₂ exhibits an original three-dimensional network of two tin atoms occupying independent crystallographic sites Sn1 and Sn2. Moreover both Sn atoms show different coordination type with fluorine atoms both distorted and one-sided, Sn1 with CN = 4 + 1 making a fluorine triangular bipyramid Sn1F₄E1 the lone pair sitting at the apex of equatorial triangle, while Sn2 with CN = 5 + 1 exhibits an octahedron Sn2F₅E2, E2 being at opposite apex of the summit of the fluorine square pyramid. A perspective view of α SnF₂ along [010] is

Table 4X-ray [12] and DFT-ELF data of γ SnF₂E.

γ SnF ₂ E - [12] Tetragonal - Space group P4 ₁ 2 ₁ 2 (N°92)						
Phase transition ~460K. - Molecular weight: 156.686 - $\rho_x = 4.64(\text{g}/\text{cm}^3)$.						
	a (Å)	b (Å)	c (Å)	V (Å ³)	Z	V(F,E) (Å ³)
X-ray [3]	5.0733	5.0733	8.4910	218.54	4	18.2
DFT-ELF [pw]	5.130	5.130	8.516	224.12	4	18.7

Interatomic distances (Å) and angles (°) - DFT - ELF analyses -* average						
Sn-Fa, Fb eq	2.115	Fc-Fa = Fd-Fb	2.911	\angle Fa-Sn-Fb eq	91.3	
Sn-Fc, Fd ax	2.327	Fc-Fb = Fd-Fa	2.907	\angle Fc-Sn-Fd ax	156.1	
Sn-E	0.97	E-E	3.530			
E-Feq	2.878	E-Fax	2.700	Mean E-F*	2.789*	
E ellipsoid a/b/c	1.24/1.14/0.95		rE	1.103		

eq:equatorial; ax: axial. F* equatorial for averages.

Coordinates: E: 0.6367/0.3633/0.25. Sn: 0.5029/0.4971/0.25. F: 0.1375/0.2643/0.1691.

E a/b/c ellipsoid size - rE: the radius of the sphere of influence.

given in Fig. 5.

All coordination details of both Sn1 and Sn2 are summarized in Table 2 and each polyhedron is shown in the right part of Fig. 5. Sn1 exhibits a triangular bipyramid (TBP) Sn1F₄E1 with four fluorine atoms one-sided and a lone pair E1 at the apex of the equatorial plane (F2F3cE). The TBP Sn1F2F3cF4aF3iE2 shows two strong covalent

equatorial bonds as reported in Table 2 delimitating the equatorial base (average Sn1-F* = 2.080 Å), one axial bond Sn1-F4a being slightly bigger (+0.08 Å) than Sn1-F* while the second Sn1-F3i introducing more distortion with 0.52 Å elongation. The lone pair E1 with Sn1-E1 = 0.862 Å appears slightly below the equatorial plane Sn1F2F3c and the average distance E1-F* = 2.73 Å.

Sn2 with its lone pair E2, is outside a square pyramid formed by five fluorine atoms F1apF1F2F3F4, the lone pair E2 being opposite to the apical fluorine (F1ap) (\angle E2Sn2F1ap = 175.2°). Sn2 below the base of the square pyramid is inside a distorted octahedron.

Four Sn and four F atoms are formed around twofold A2 axis a fourfold ring [Sn₄F₄] shaded in yellow for clarity. α SnF₂ develops a tunnel along [010] occupied by E2 lone pairs, E1 being close to its wall. It also designs the skeleton of [Sn₄F₈] tetramer which results from solid SnF₂ sublimation. Worthy to note that [Sn₄F₄] rings are held together along [100] and [010] by fluorine corner-sharing F1, F1ap, F3 and F3i of the Sn2F₅E2 octahedra and along the third direction by a couple of Sn1F₄E1 triangular bipyramids sharing an edge F3c-F3i also corner shared with Sn2F₅E2 octahedra.

4.1.1. Electron localization function

Looking to lone pairs Sn1-E1 and Sn2-E2 distances a deformation of the first one is noted which can be related to its surrounding being squeezed close to the center of symmetry in a quadrilateral tunnel formed along [010] by F2F4aF3cF3i.

E1 lone pair domain, marked by its electronic cloud covers Sn1; it appears “blown” towards F3c direction by fluorine network (Fig. 6a). Therefore sections based on Sn1, E1 and associated fluorine atoms of equatorial and axial planes of TBP (Sn1F2F3cF4aF3iE2) have shown in

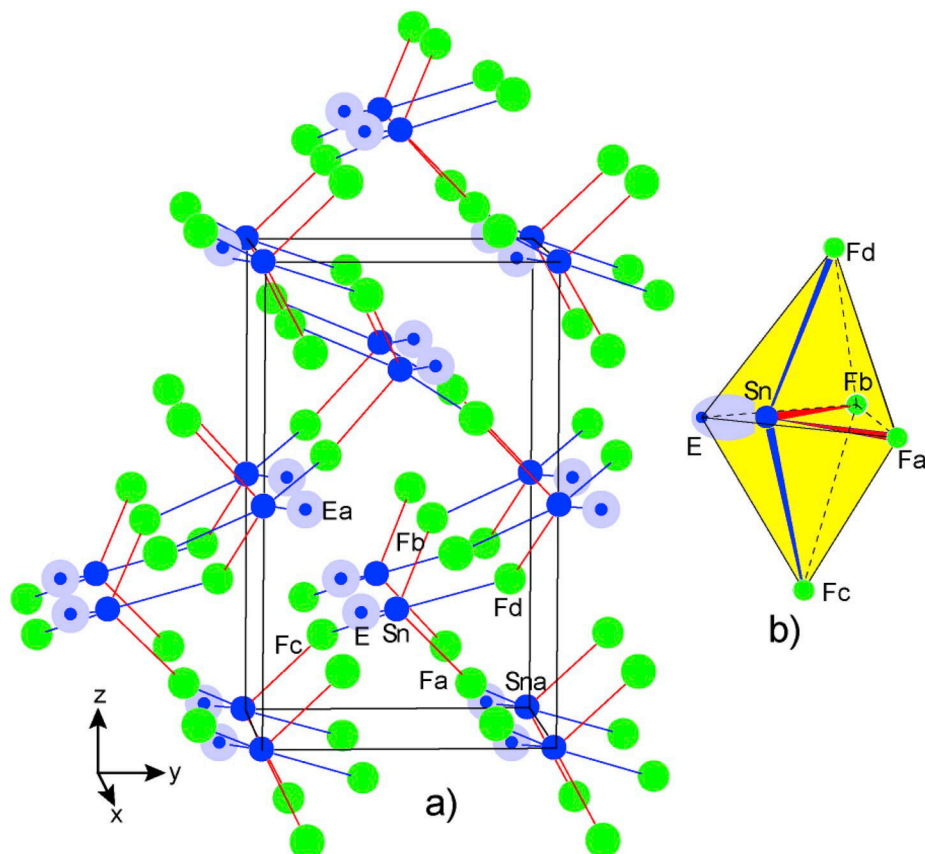


Fig. 10. a) View of γ SnF₂ three-dimensional network built up by [SnF₄E] TBP's sharing all fluorine apices; b) Detail of one-sided coordinated Sn atom to fluorine atoms making a triangular bipyramid [SnF₄E] (equatorial bonds in red). (For interpretation of the references to color in this figure legend, the reader is referred to the Web version of this article.)

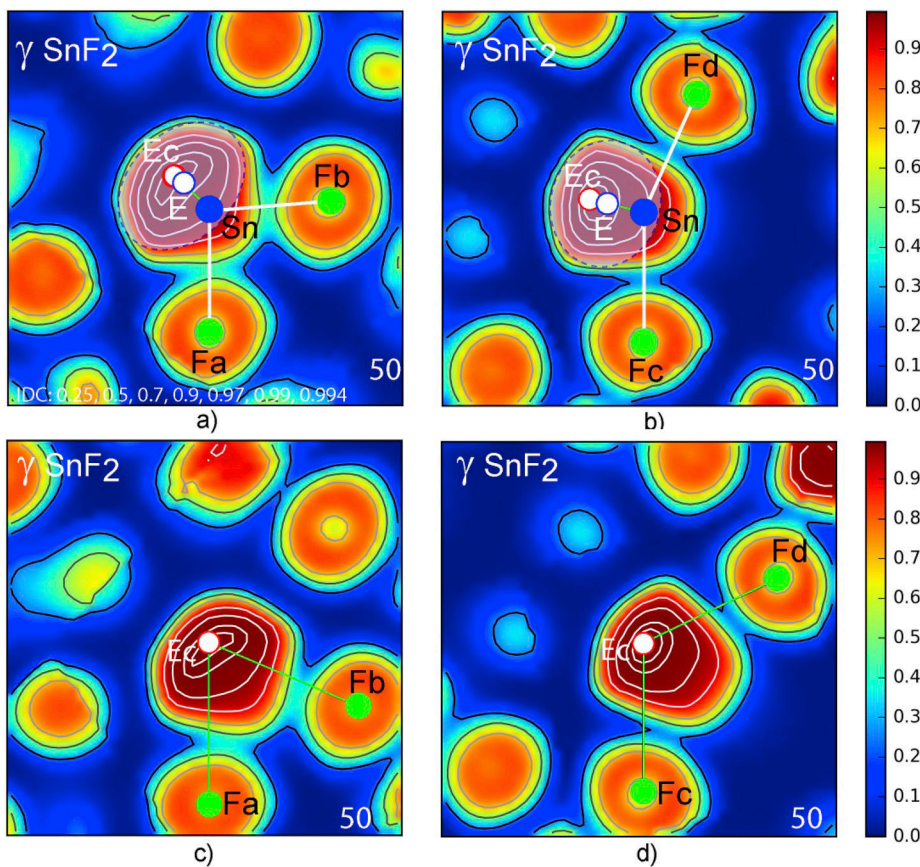


Fig. 11. γ SnF_2 . **a) b)** ELF sections showing the electronic density of equatorial and axial planes of SnF_4E TBP. E (white blue circle) marks the center of the elliptic section of the electronic cloud around the lone pair core Ec (max. isodensity curves IDC – white red circle). **c) d)** Sections EcFaFb and EcFcFd allow to check the Ec coordinates and to show two sections at 90° showing the influence of F atoms on the electronic cloud testifying its plasticity. Refinement of Ec coordinates shows a perfect set up with isodensity curves. (For interpretation of the references to color in this figure legend, the reader is referred to the Web version of this article.)

these ELF sections the possibility to settle E1. We notice that E1 (blue ring) is clearly displaced from Ec1 (red ring) by $\text{Ec1-E1} = 0.55 \text{ \AA}$. A similar analysis has been done using axial plane Sn1F4aF3i (Fig. 5c). It is worth to note that the electronic cloud around E1 is less disturbing in that direction and that its E1 gravity center coils are closer to Ec1. The size of E1 with its electronic cloud is concentrated and deformed in a large ellipsoidal volume, giving a volume of influence $\text{rE1} = 1.05 \text{ \AA}$, almost the size of a fluorine atom.

E2 on its own does not show in sections reported in Fig. 7 same constraints inside the endless tunnel delimited by $[\text{Sn}_2\text{F}_4]_n$ tetramer ring along [010], then E2 size corresponds to an ellipsoid of roughly the same sphere of influence size $\text{rE2} = 1.06 \text{ \AA}$ (cf. Table 2). To extract the E2 dimensions the diagonal planes of the fluorine square pyramid Sn2F2F3 and Sn2F1F4 of the Sn2F1apF1,2,3,4E octahedron have been calculated (Fig. 3a,b,c,d) two other sections were also particularly interesting SnEc2F1ap and Ec2F2F4 plane. They are reported in Fig. 7 and analyzed alike previously. Fig. 7e and f are detailed showing the Ec2 LP center (red circle) in its electronic cloud (pale transparent blue ellipse). Fluorine atoms F1ap and F2, F4 of the tetramer link with Sn2 exhibit a solid bonding (2.048, 2.197, 2.276 \AA), while the remaining ones F1 and F3 engaged to connect with the next tetramer ring via Sn2c and Sn1a (2.386 \AA and 2.494 \AA), show a small rupture of the electron density (see Fig. 7).

4.2. β SnF_2

The synthesis mode needed to obtain β SnF_2 leads to a metastable

phase. Its structure was determined and refined using X-ray powder pattern data [11] (Table 3 and Fig. 8). Therefore taking advantage of this piece of information a refinement of the network was realized using DFT-ELF calculations. The results showing a little condensation of the network and various interatomic distances are reported in Table 3.

In β SnF_2 there is one independent Sn atom bonded to five F making a distorted quadrilateral pyramid (Fig. 8). Taking into account its lone pair E, CN = 5 + 1 coordination $[\text{Sn}_5\text{E}]$ occurs in the form of a distorted octahedron, particularly its equatorial plane F2bF2cF1a (Fig. 9a & f). As usual, the shortest Sn–F1ap bond (red stick) extends towards the apex of the fluorine square pyramid and all the angles are in between $73.8^\circ \angle \text{F1-Sn-F2b,F1a}$, $\text{F2} < 83.7^\circ$ but the angle $\angle \text{F1-Sn-F2c} = 104.0^\circ$ thereby reflecting the pronounced puckering of the equatorial plane, the dihedral angle $\text{F1a-F2bF2c-F2c} = 23.8^\circ$. After locating E one finds that $\text{Sn-E} = 1.019 \text{ \AA}$, a value very close to the one of Sn2 in α SnF_2 having the same octahedral coordination with $\text{Sn2-E2} = 0.987 \text{ \AA}$. The $\text{Sn-F1ap} = 2.131 \text{ \AA}$, apical bond in β SnF_2 , is slightly bigger than in α SnF_2 (2.048 \AA) and averaged Sn–F distances of the equatorial plane are similar 2.379 \AA against 2.337 \AA .

A projection of the structure along [010] shows, alike in α phase, a kind of fourfold ring making a tunnel along [010] (Fig. 9b). Its section shaded in pale green color looks like the yellow one of the α phase, therefore two Sn–F1ap bonds participate to bordering the tetramer while they were uniquely engaged in interconnecting bonding previously. It is also noted that two lone pairs E point towards the inside of the tunnel where they find enough space, $\text{Ec} \dots \text{Eb} = 2.941 \text{ \AA}$. Repeated by the twofold screw axis they design an endless double chain along

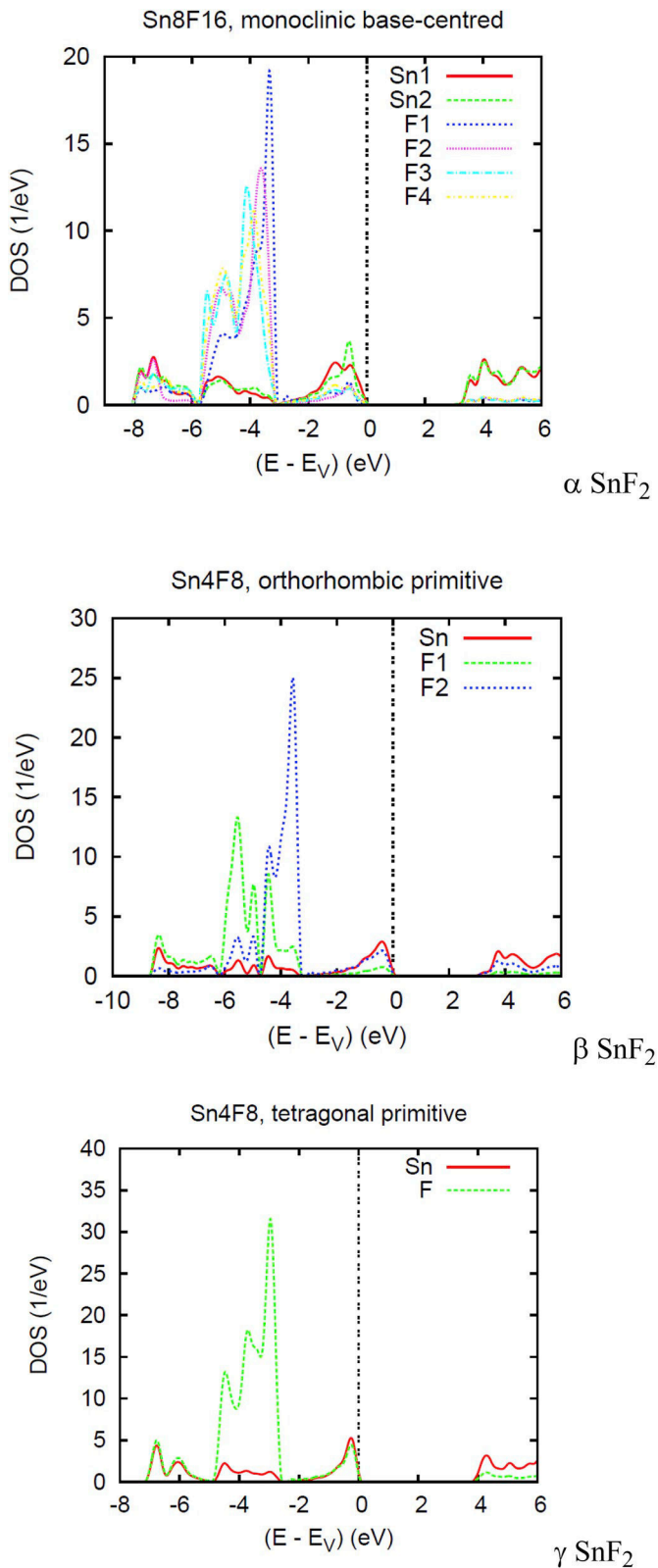


Fig. 12. Site projected density of states (DOS) of divalent tin fluoride Sn^{II}F₂ three varieties.

[010].

Each [SnF₅E] octahedron share corners with five other octahedra thereby creating a three-dimensional network as illustrated in Fig. 9a. There is a strong connection between Sn and Sn_c via Sn-F_{1ap} = 2.131 Å and Sn_c-F_{1a} = 2.336 Å bonds. They show around the twofold screw axes located in $y = 1/4$ and $3/4$ and parallel to [010] a condensation of the network which leaves along this direction a channel in which lone pairs chains extend. The average distance of E with surrounding fluorine atoms making a distorted quadrilateral is 2.756 Å.

4.2.1. Electron localization function

A series of sections in ELF data allowed appreciating the nature of bonding. All Sn-F bonds appear well associated with F by covalent bonding but Sn-F_{2c} = 2.668 Å, longer than the four others Sn-F_{1ap}, F_{1a}, F₂, F_{2b}, and therefore more relevant of ionic-covalent character (Fig. 9b and d). The coordinates of the E_c core of Sn lone pair (little red circle) have been refined in Fig. 9a,b,c,d sections.

Fig. 9e is a section by a plane containing three E immediate neighbors of E_c; showing that they are free of constraints. An ellipsoidal (a/b/c) envelop for E has been determined (see Table 3) E_c being accompanied by an electronic cloud, giving finally a sphere of influence with radius $r_E = 1.013$ Å. Its center (little blue circle) as ever is slightly off E_c position (0.2–0.3 Å) its plasticity being sensitive to the various network interactions.

4.3. γ SnF₂

X-ray powder data needed to determine the structure of this γ SnF₂ phase were collected after heating at 190 °C, followed by slow cooling down to 80 °C, where the temperature was maintained to stabilize this variety of tin II fluoride (Table 4).

The salient feature of the γ SnF₂ structure is a new change of Sn II to coordination polyhedron CN = 4 + 1, a triangular bipyramid (TBP) [SnF₄E] alike Sn1 in α SnF₂. This TBP as shown in Fig. 10a is the one-sided coordination of Sn with four Fs, the lone pair E at the apex of the equatorial triangle making up the triangular bipyramid. Equatorial bonds Sn-F_a, F_b (red sticks in Fig. 10), equivalent by symmetry 2.115 Å, are slightly bigger than mean Sn1-Fe_q = 2.080 Å of α allotrope while the two Sn-F_{ax} = 2.327 Å are very different in α phase alike ∠F_a-Sn-F_b equatorial (91.3°) and ∠F_c-Sn-F_d axial (156.1°) angles are more open instead of 86.7° and 142.7° due to strong E-bond pairs repulsions. Sn-F_c, F_d are longer than the equatorial ones by 0.2 Å, a value already found in such type of [MⁿX₄E] TBP (X = O or F). Each [SnF₄E] TBP shares apices with four different homologs. Equatorial apices are systematically linked to axial ones, the short bond being followed by a longer one; for example, Sn-F_a-Sn_a with Sn-F_a = 2.132 Å and F_a-Sn_a = 2.323 Å, F_a equatorial for Sn becomes an axial F for the [SnF₄E] TBP. Such a bonding scheme generates a three-dimensional network as illustrated in Fig. 10b in which, as in the previous allotropic phases a large rectangular tunnel can be seen parallel to [100], defined here by a pseudo ring {Sn₆F₆}, a tunnel which welcomes the lone pairs of tin II (see Fig. 11).

4.3.1. Electron localization function

Opposite to α and β the γ SnF₂ variety does not show a CN = 6 in form of [SnF₅E] octahedron but to the triangular bipyramid CN = 5 alike the one centered on Sn1 of α form. Both Sn-F equatorial and axial bonds show IDC continuity indicating a stable SnF₄E₂ unit in this three-dimensional network.

The density maximum close to Sn atom is shown in Fig. 11 by a little white-red circle which gives E_c centroid of the lone pair. The associated electronic cloud with its E center (white-blue circle) is delimited and

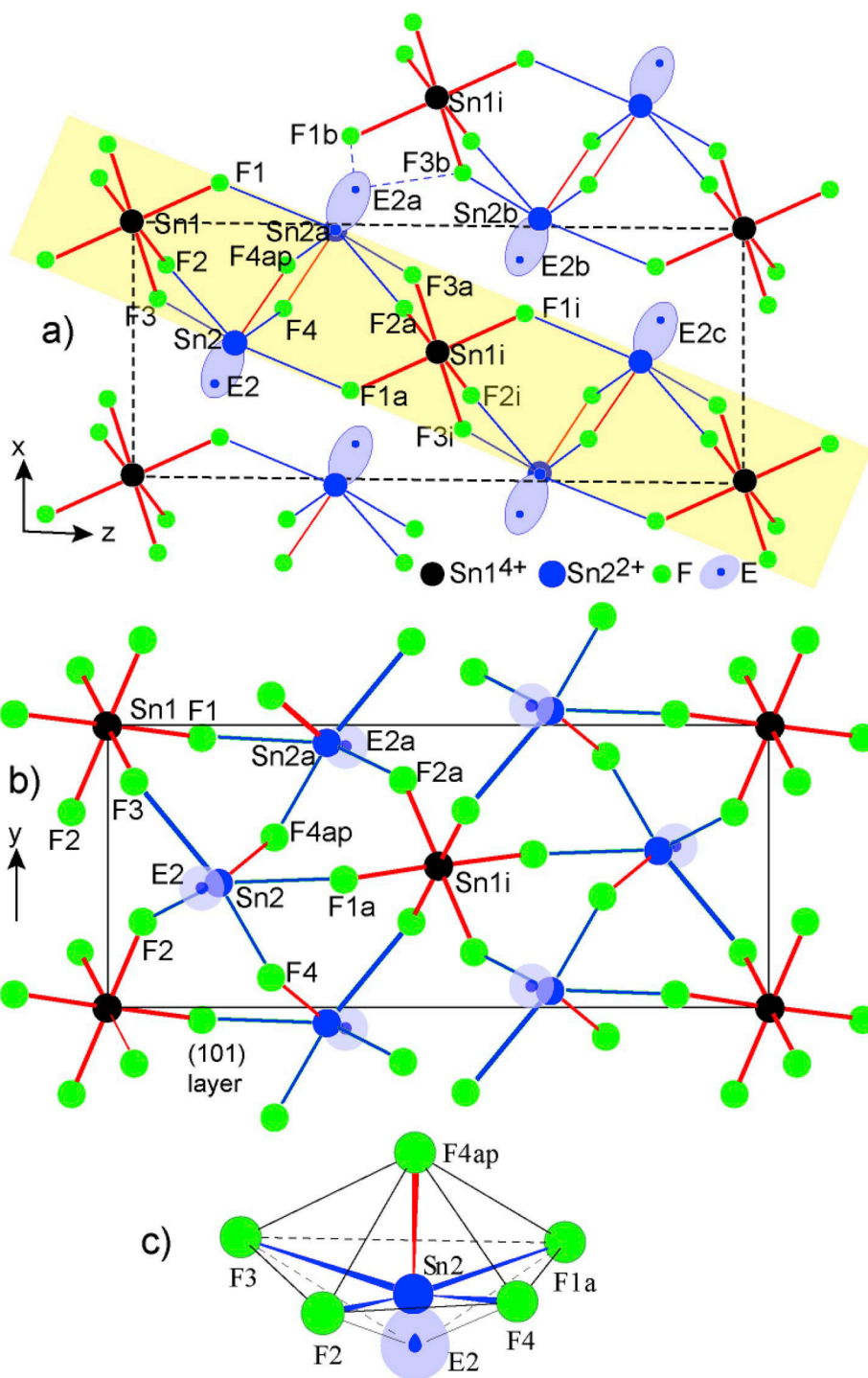


Fig. 13. a) Projection onto $[010]$ plane of the $\text{Sn}_3\text{F}_8\text{E}_2$ crystal structure. Sn^{4+} and Sn^{2+} are shown in black and blue circles, $\text{Sn}^{4+}\text{-F}$ and $\text{Sn}^{2+}\text{-F}$ bonds in red and blue sticks, E in a pale blue ellipse. The $[\text{Sn}_3\text{F}_8\text{E}_2]$ layer formed by Sn^{4+}F_6 and $\text{Sn}^{2+}\text{F}_5\text{E}$ octahedra F corner shared is parallel to (101) plane (shaded in yellow); worthy to note that a double plane of E separate $[\text{Sn}_3\text{F}_8\text{E}_2]_n$ layers. b) Detail of an isolated $[\text{Sn}_3\text{F}_8\text{E}_2]_n$ layer, parallel to (101) plane, showing the endless zigzag string of $\dots \text{Sn}2\text{-F}4\text{ap-Sn}2\text{-F}4\text{ap} \dots$ along $[010]$. c) Perspective view of the $\text{Sn}2\text{F}_5\text{E}$ distorted octahedron. (For interpretation of the references to color in this figure legend, the reader is referred to the Web version of this article.)

Table 5X-rays [6] and DFT-ELF (pw) data of SnSn₂F₈E₂.

Sn ₃ F ₈ - [6] Monoclinic - Space group P2 ₁ /n (N ¹⁴) - Molecular weight: 508.06 g ρ _x = 4.86 (g/cm ³).									
	a (Å)	b (Å)	c (Å)	α (°)	β (°)	γ (°)	V (Å ³)	Z	V(F,E) (Å ³)
X-rays	5.2155	5.3208	12.483	90	90.38	90	345.97	2	19.3
DFT-ELF [pw]	5.217	5.318	12.473	90	90.36	90	346.04	2	19.3
Interatomic distances (Å) and angles (°) - [Sn ⁴⁺ (Sn1) - Sn ²⁺ (Sn2)]									
Sn1-F1 (x2)	1.960		Sn2-F4a ap	2.097		F4a.ap-Sn2a	2.169		
Sn1-F2 (x2)	1.977		Sn2-F4	2.169		Sn2-F1a	2.555		
Sn1-F3 (x2)	1.951		Sn2-F2	2.253		Sn2-F3	2.651		
Sn2-E2	0.938		E2a-F1b	2.721		∠ESn2F4ap	157.7		
E2-F2	2.761		E2a-F3b	2.578		∠F4apSn2F*	80.4 ± 5.2		
E2-F4	2.675		E2a-E2b	3.900		∠E2Sn2F1a	89.1		
E2b-E2c	3.989		Mean E-F	2.766		∠E2Sn2F3	100.3		
E ellipsoid a/b/c			1.15/1.10/0.90			rE	1.04		

eq.: equatorial; ax: axial. F* equatorial averages. E a/b/c ellipsoid size.

Coordinates: E: 0.3600/0.5743/0.1407 - rE: sphere of influence.

marked by a dotted pale blue ellipse. E is moved out from Ec by ~ 0.3 Å because interactions of network requesting its plasticity.

4.3.2. Electronic density of states of the three Sn(II) fluorides

The site projected electronic density of states DOS is shown for the three SnF₂ varieties in Fig. 12. Along the x-axis, the energy zero is at the top of the valence band VB, separated from the conduction band CB by a large bandgap. Then SnF₂ is insulating in its three phases.

The bandgap magnitude increases along with the series going from ~ 3 eV for α SnF₂ then ~ 3.3 eV for β SnF₂ and ~ 3.8 eV for γ SnF₂. The change of bandgap magnitude is likely due to the different local surroundings of Tin as shown in Figs. 5, 8 and 10.

The energy low lying F-s states are not taken into account in the explicit basis set. This is also the case of full Sn 4d¹⁰ states.

From this, Sn explicit basis set is of s and p character while F valence states are of p character. Due to the large filling of F p subshell (F is 2p⁶-like) the F PDOS are of large intensity and are found dominating VB. The Sn s and p states mix with those of F p to ensure for the bonding. Within the valence band, the similar DOS skylines indicate the quantum mixing between the valence states. This is particularly so for the extent of the VB up to its top. Note the different DOS of the two Sn sites in the α phase due to the local surrounding of Sn1/Sn2 detailed in Fig. 5.

5. Tin (II-IV) mixed-valence fluorides

5.1. Sn₃F₈ or Sn₂²⁺Sn⁴⁺F₈E₂

Single crystals of this tin fluoride were obtained by direct oxidation of an HF solution of SnF₂. After analysis using various techniques, in particular, Mössbauer spectroscopy, the mixed valent formula of this fluoride was precisely established as Sn₂²⁺Sn⁴⁺F₈ [23]. Following the introduction into a glass capillary, the X-ray analysis showed that it belongs to the monoclinic system (Table 4).

Tin atoms are located on two crystallographic sites, Sn1 which accommodates Sn⁴⁺ onto symmetry center, Sn²⁺ being on Sn2 site. A projection of the framework onto (010) plane is given in Fig. 13a.

Sn1⁴⁺ with six fluorine atoms creates a flattened Sn1F₆ octahedron sharing all these apices with six independent Sn2²⁺ ions (Fig. 13b). The Sn1-F1,2,3 are quasi identical at 1.963 ± 0.013 Å. Note the major differences with Sn-F_{ax} = 1.874 Å bonds which assume the connection into endless [SnF₄]_n strings and free Sn-F_{eq} = 2.025 Å bonds in SnF₄ fluoride.

Sn2²⁺ exhibits a sterical active lone pair and a CN = 5 + 1 coordination in the form of an octahedron Sn2F₅E (Fig. 13c). Sn2-E2 = 0.938 Å is in agreement with previous cases therefore smaller than Sn2-E2 = 0.987 Å in α SnF₂E and Sn-E = 1.019 Å in β SnF₂E.

These Sn2²⁺F₅E octahedra are associated along [010] by F4p atoms along [010] developing an endless zigzag string ... Sn2-F4ap-Sn2-F4ap ... the remaining fluorines F1, F2 and F3 assuming the layer formation by interconnection with Sn1F₆ octahedra. Such bonding develops an [Sn₃F₈E₂]_n layer parallel to the plane (101). E lone pairs border these layers filling the interspace between them via a double layer, van der Waals interactions assuming the stability of the packing. In this space, the closest interatomic distances between consecutive layers are E2-F1b = 2.708 Å and E2-F3b = 2.966 Å while F-F distances are above 3 Å as well as Sn2a-F1 or F3i making an improbable weak interaction. So the stability of Sn₃F₈ framework appears to be provided via lone pair-fluorine inter-actions.

An isolated [Sn₃F₈E₂]_n layer is shown together with the distorted [Sn2F₅E] octahedron (O) in Fig. 13b and c. One can see that [Sn2F₅E]_n make infinite zigzag strings along [010] by corner-sharing of their equatorial apices; they are held together by Sn1F₆ octahedra. Note the twofold role of E which, at the level of the [Sn2F₅E] (O), via the strong repulsion lone pair-bond pair, pulls down the angles $\angle F4apSn2F^*$ to 80.4° and $\angle ESn2F4ap$ to 157.7° and which at the level of the framework holds together [Sn₃F₈E₂]_n layers via E - F interactions. Note also the bond lengths of Sn2-F1a and Sn2-F3 and angles E2Sn2F1a and E2Sn2F3 which are impacted by E pair-bond pair repulsion (Table 5).

5.1.1. Electron localization function ELF

A series of sections in ELF data allows determining E coordinates and also lone pair shape in Fig. 14. The distance Sn2-E is closed to preceding values found for α and β SnF₂. The E electronic volume,

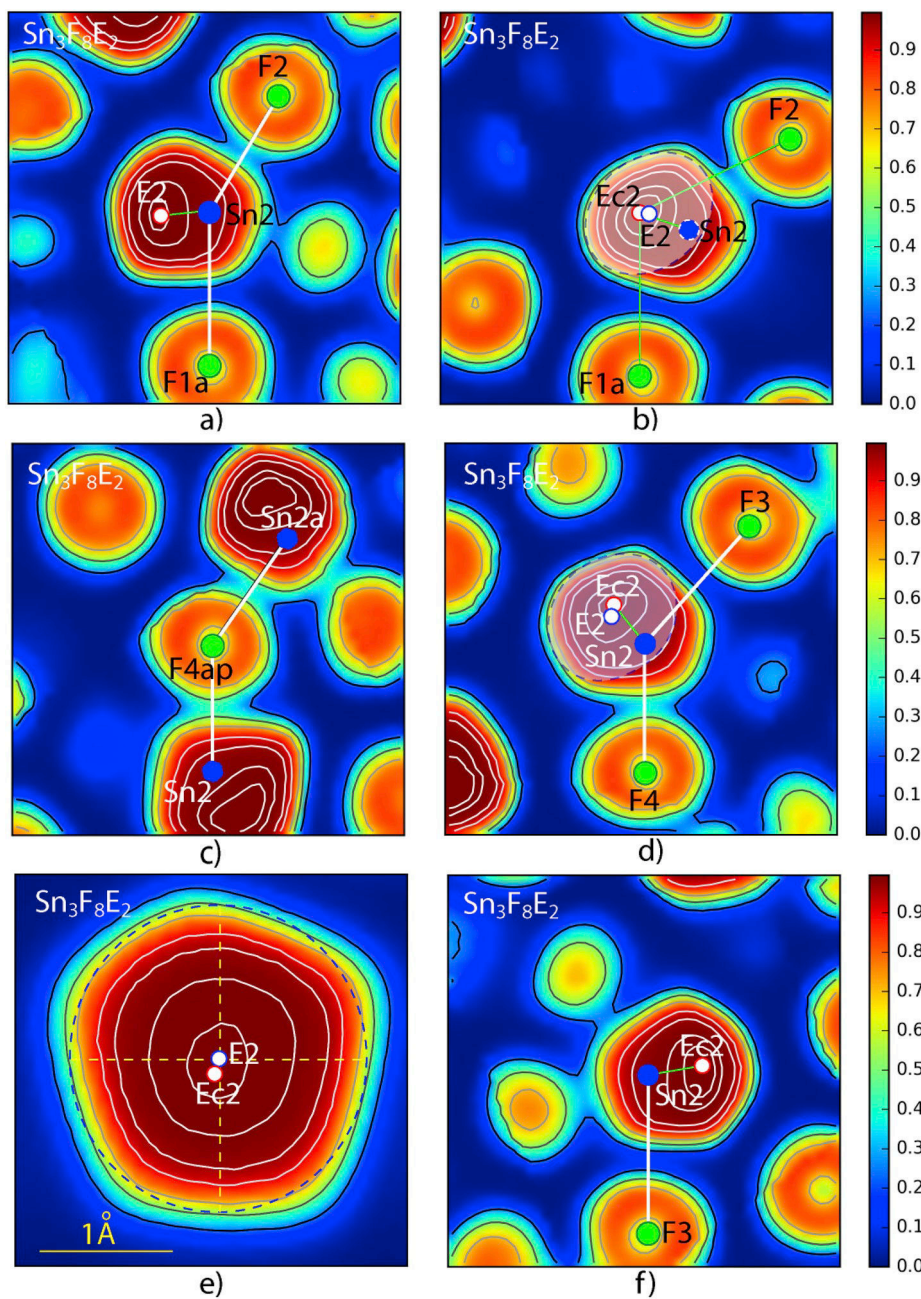


Fig. 14. ELF of $\text{Sn}_3\text{F}_8\text{E}_2$. **a)** Sn2 via Sn2–F1a and Sn2–F2 equatorial bonds assume the bridging between two ($\text{Sn}1\text{F}_6$) octahedra (see Fig. 13a and b) a section of Sn2 lone pair is clearly marked; **b)** this section based on the same fluorine atoms F1a and F2 and Ec2 electron density maximum of E2 lone pair allows determining two parameters of E2 ellipsoid. **c)** F4ap strongly tightens the thickness of $[\text{Sn}_3\text{F}_8\text{E}_2]_n$ layer. **d)** The section Sn2F4F3 almost at 90° of **b)** offers the possibility to check again E2 shape. **e)** E section by a plane perpendicular in Ec to Sn2–Ec2 vector shown in **f)**.

which always accompanies the core Ec of the lone pair, has been determined to make at the summit of $\text{Sn}2\text{F}_5\text{E}$ octahedron a helmet density on Sn2. Therefore owing to various repulsive interactions the $\angle\text{FSn}2\text{F}$ angles of the octahedron have been somewhat shackled. Anyhow the various sections show a large coherence with crystal data as shown in Fig. 14.

They show that Sn2–F1a bond is not covalent like Sn–F2 but it

participates in layer coherence by bridging two $\text{Sn}1\text{F}_6$ octahedra along $[\bar{1}01]$ (Fig. 14a).

In Fig. 14b, E2F1aF2 allows us to determine Ec2 coordinates of lone pair and to draw its elliptic section (pale blue color) and to precise its center (blue-white circle) slightly distant from Ec $< 0.02 \text{ \AA}$. Fig. 14c shows the link between to Sn^{2+} and Sn^{2+} , i.e. Sn2–F4ap–Sn2a, in fact, doubled by Sn2a–F4–Sn2 fixing strongly the thickness of $[\text{Sn}_3\text{F}_8\text{E}_2]_n$

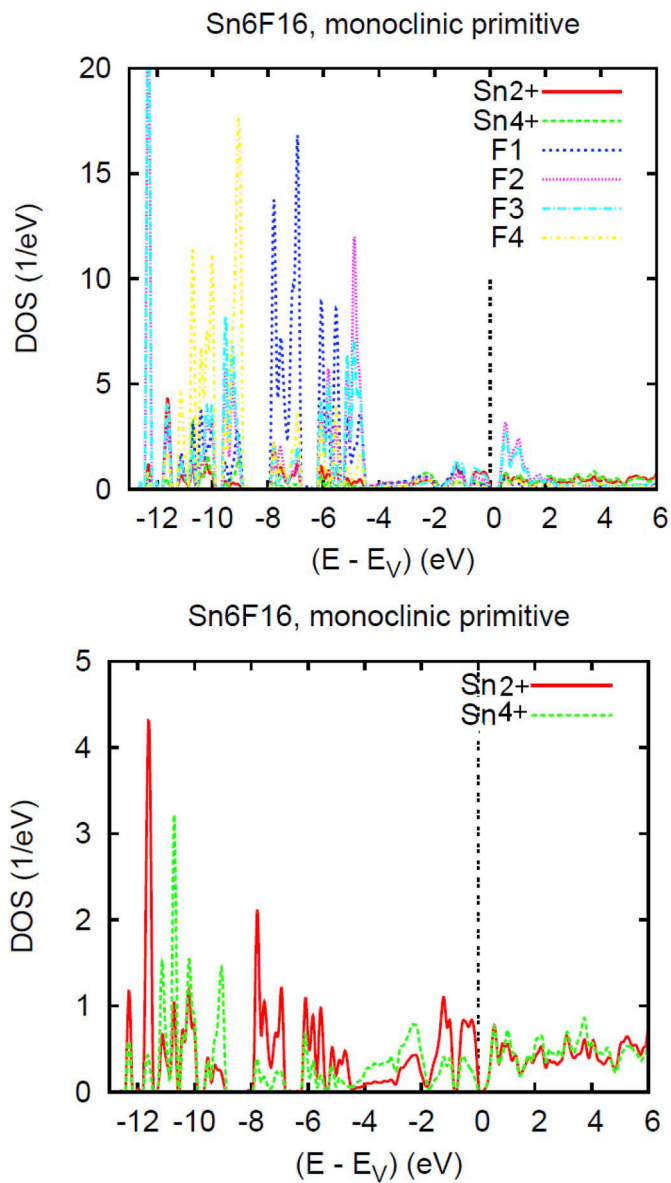


Fig. 15. Sn_3F_8 (Sn_6F_{16}): Site projected DOS with all constituents (top) and focus on the $\text{Sn}^{2+}/\text{Sn}^{4+}$ partial DOS (bottom).

layer. The network of this layer is the result of an endless double zigzag string [... $\text{Sn}2\text{-F}4\text{-Sn}2\text{-F}4\text{ap-Sn}2\text{a}$...]_n parallel to [010] (b periodicity) associated by $\text{Sn}1\text{F}_6$ octahedra in (101) plane, repeated with $c/2$ periodicity, making endless piling along [010] [... $[\text{Sn}1\text{F}_6]\text{-empty trigonal antiprism-}[\text{Sn}1\text{F}_6]$...]_n. The E's produce not only distortions on $\text{Sn-F}_{1,2,3}$ bonds but also, with their double plane between the layers, they assume their packing by Van der Waals-like interactions.

5.1.2. Site projected density of states

The site project DOS of Sn_3F_8 is shown in two panels in Fig. 15. Due to a large number of fluorine sites the valence band VB has a rather complex character but it is clearly dominated by the F p states (low

energy s states not shown). F-p is prevailing from -12 to -6 eV within VB and shown some bonding (similar skylines) with the two Sn valences.

The gap between VB and CB is very small, which is concomitant with the mixed-valence compound. Focusing on the Sn states is shown on a smaller scale DOS at the lower panel. Clearly, the simultaneous presence of divalent and tetravalent Sn leads to a reduced bandgap. Sn^{2+} with two lone electrons than Sn^{4+} has the PDOS larger throughout the VB and especially at the top of the VB. However, there can be noticed differences of magnitudes such as in the $-4,-2$ eV energy window, where Sn^{4+} PDOS are larger. This translates complex bonding features with F substructures illustrated above in the ELF maps.

5.2. Sn_2F_6 or $\text{Sn}^{2+}\text{Sn}^{4+}\text{F}_6$

This second mixed-valence fluoride was obtained by direct synthesis of stoichiometric SnF_4 and SnF_2 . It is sensible to moisture. It crystallizes in the cubic system as revealed by neutron diffraction patterns (Table 6). Its structural network is simply a doubling of the well known ReO_3 structure, therefore, evidencing an order between Sn II ($\text{Sn}1$) and Sn IV ($\text{Sn}2$) [7]. A view of the structure is given in Fig. 16a and b.

The main feature of this di-fluoride is a marked difference in the volume of octahedra $\text{Sn}1^{2+}\text{F}_6$ (16.2 \AA^3) and $\text{Sn}2^{4+}\text{F}_6$ (13.0 \AA^3) and to find Sn^{2+} and its lone pair E together onto a symmetry center. This particular situation can be related to the relativistic effect due to important electron speed at such a high atomic number: $Z_{\text{Sn}} = 50$ and the space provided by the large fluorine octahedron of the network. In this particular case, the centroid E_c of the lone pair is at its maximum velocity transforming Sn^{II} in a large cation $[\text{SnE}]1^{2+}$ roughly analogous to Sr^{2+} for example. Based on $r\text{F}^- = 1.19 \text{ \AA}$, $r[\text{SnE}]1^{2+} \sim 1.11 \text{ \AA}$ a size smaller than $[\text{SnE}]3^{2+} \sim 1.30 \text{ \AA}$ (close to Ba^{2+}) in the fluoride cube of the mixed-valence oxyfluoride $[\text{SnE}]^{2+}\text{Sn}_3^{4+}\text{O}_2\text{F}_{10}$ [25], allowing to appreciate the constraints of an octahedral surrounding against a hexahedral one, therefore showing also the plasticity of the sphere of influence of E.

Again in this double ReO_3 type unit, there are empty distorted cuboctahedra. The square faces are now rectangular, two opposite faces being in anti position. The trigonal faces have edge lengths corresponding to those of $[\text{SnE}]1\text{F}_6$ and $\text{Sn}2\text{F}_6$ octahedra. The distances between its center marked by the star to the twelve fluorine atoms amount to 2.950 \AA ; it suggests that a large cation like Ba^{2+} could be introduced giving eventually non-stoichiometric mixed-valence phases $\text{Ba}_x[\text{SnE}]_{1+x}\text{Sn}_{2-x}\text{F}_6$.

5.2.1. Electron localization function ELF

$[\text{SnE}]1\text{-F}_6$ bonds are 0.433 \AA bigger than $\text{Sn}2\text{-F}$ ones showing for the former ionic interactions while the second shows clearly covalent character. Anyhow it is interesting to have a look also onto the particular case of the lone pair triplet of the fluorine atom sandwiched by $[\text{SnE}]1$ and $\text{Sn}2$. Fig. 17 gives some data on both Sn^{II} and Sn^{IV} cations and lone pair triplet of F.

Fig. 17a shows a planar section $\text{Sn}1\text{FaFb}$ of ELF data. A large high electron density curves appear concentrated onto $\text{Sn}1$ crystallographic site testifying that Sn^{II} and its E ($5s^2$) lone pair make a unique large cation $[\text{SnE}]1^{2+}$. Fig. 17b shows a drastic difference; the bonding $\text{Sn}2\text{-F}_4$ is marked its association showing directly its impact on F density curves. Note that maximum intensity IDC = 0.83 underlined by a white red circle in the two "crescent moon density" (IDC = 0.80) open by $\text{Sn}2\text{-F}$ bond indicate respectively the centroid E_{ca} trace (section of

Table 6
Crystal data of Sn₂F₆E.

Sn ₂ F ₆ E - [6] Z Anorg. Allg. Chemie, 590, 173–180, 1990.								
Cubic, Space group Fm $\bar{3}$ m (N ^o 225), Molecular weight: 351.37, $\rho_x = 4.05$ (g/cm ³).								
a (Å)	b (Å)	c (Å)	α (°)	β (°)	γ (°)	V (Å ³)	Z	V(\square ,F) (Å ³)
8.321	8.321	8.321	90	90	90	576.1	4	18.0
Interatomic distances (Å) and angles (°) [Sn ²⁺ (Sn1) – Sn ⁴⁺ (Sn2)]								
[SnE]1-F (x6)	2.297			Sn2-F (x6)	1.864		\square - F (x12)	2.950
F-F (oct. [SnE]1) (x12)	3.248			F-F (oct. Sn2) (x12)	2.636			
[SnE]1-Ea	2.237			Sn2-Ea	2.068		Fa-Ea	0.566
[SnE]1-CT	2.167			Sn2-CT	1.993		CT-Fa	0.129
T. rd.rect.Fa	2.13/1.50/0.65			\odot Text.{F2E2 ₃ } blue dotted circle	1.93		T.gyr. yellow circle - radius	0.552
Fig. 16 L/H/R				rE2	0.51			
Ea ellipsoid a/b/c	0.46/0.46/0.64			sphere of influence.				

eq.: equatorial. ax.: axial. Eca coordinates: x,y,z (Wy (192I) site), 0.4343/0.4913/0.7395.

CT: E2 torus center: Wy (24e) x,y,z 0.5/0.5/0.7395. T gyr. Ea: torus gyration radius.

gyration core of the electronic torus (CT center)). The associated electron cloud around Eca is somewhat displaced (white blue circle of the pale blue ellipse). Fig. 17c Then the electronic torus with its circle pathway (yellow) made by the triplet is not centered on Fa but repulsed towards [SnE]1 with Fa-CT = 0.129 Å. A little scheme of Sn₂,Fa, Ea and [SnE]1 is done in Fig. 17d.

Again it is noticed that the lone pair triplet resembling a crown, of the fluoride anion is not aligned with F center like in SnF₄ (F2-CT = 0.168 Å) where the space above CT is free, but here Fa-CT faces directly [SnE]1. So, there is a competition for the coordinate of {E₃} torus between repulsive effect of the strong bond Sn2-Fa and the ionic attraction by [SnE]1 cation which amounts only +0.129 Å giving Sn2-CT = Sn-Fa + 0.129 Å = 1.869 + 0.129 = 1.993 Å. It shows the remarkable mobility and adaptability of the {E₃} torus along the bond axis of Sn-F.

5.2.2. Site projected density of states

Fig. 18 shows the site projected density of states (DOS).

The same calculation framework as for the above-studied SnF₄, SnF₂ and Sn₃F₈ DOS have been considered especially regarding the valence basis sets of Sn and F. The valence band (VB full) is separated from the conduction band (CB empty) by an energy gap of 2 eV. The compound is thus a small gap insulator. We note here that the bandgap is smaller than in SnF₄ and SnF₂ phases but larger than in Sn₃F₈ in Fig. 15. Then mixed-valence compounds –here fluorides– are expected with smaller band gaps than single valence ones.

VB is dominated by F states (blue dotted lines) but likewise in other Sn-F studied compounds.

We further examine the bonding in view of the two different Sn valences. The lower panel of Fig. 18 shows the crystal orbital overlap population (COOP) of Sn₂F₆. For a reminder, COOPs are in shorthand notation the overlap integral S_{ij} (i and j designate two chemical species). Positive, negative and nil intensity along the COOP axis are

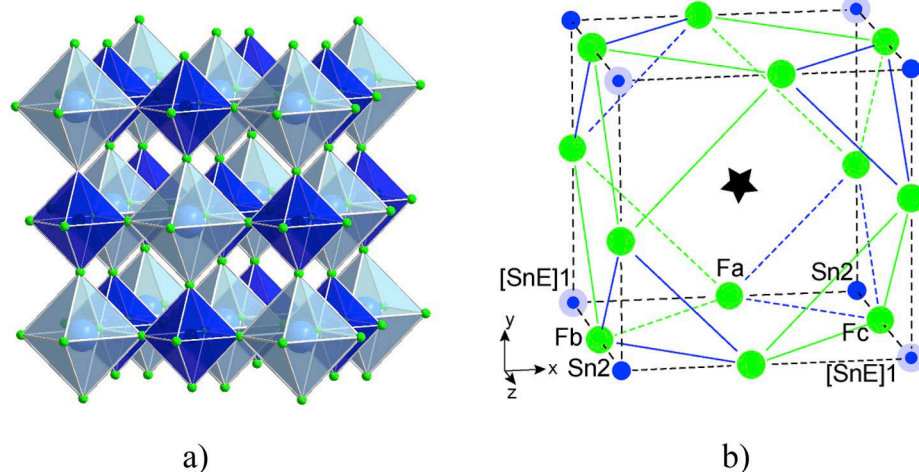


Fig. 16. a) Perspective view of Sn₂F₆E crystal network (left). Dark blue octahedra built up by fluorine atoms (green circles) receive Sn^{IV} atoms while [SnE]1^{II} large atoms, "dilated" by their lone pairs are set up in pale blue transparent octahedra. b) The sub-cube formed by [SnE]1 and Sn2 atoms show edges occupied by fluorine atoms forming an empty distorted cuboctahedron centered at 1/4,1/4,1/4, designed by a star. (For interpretation of the references to color in this figure legend, the reader is referred to the Web version of this article.)

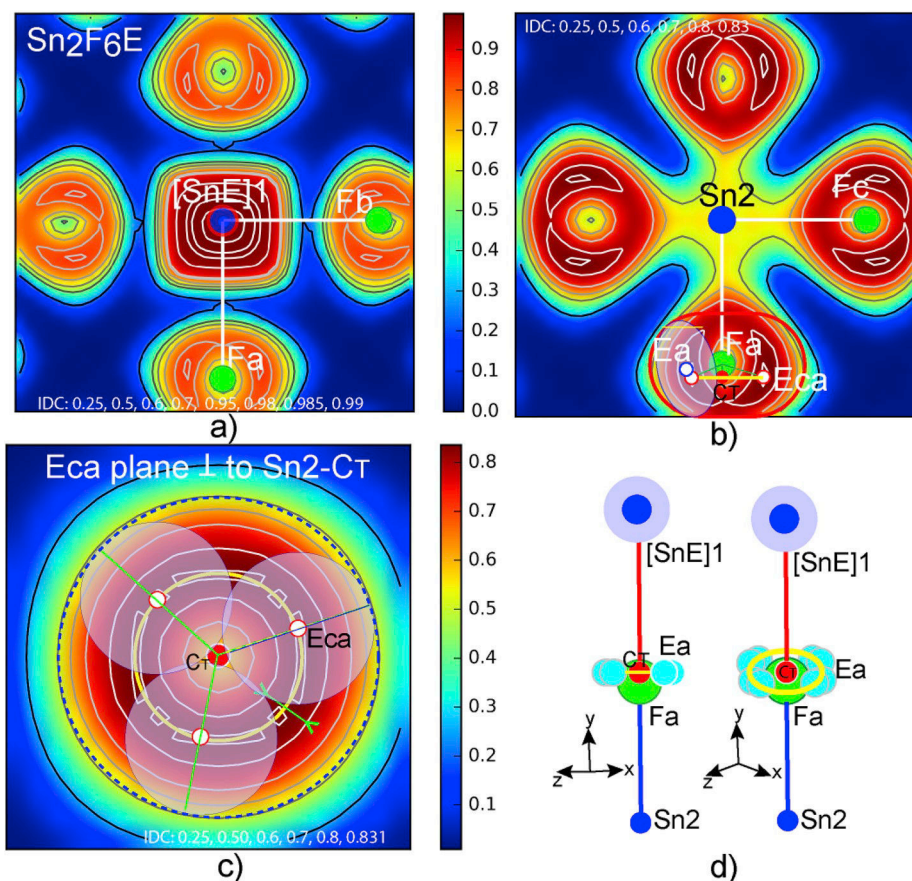


Fig. 17. a) Section $[\text{SnE}]1\text{FaFb}$ showing the diluted $[\text{SnE}]1^{2+}$ cation due to the spherical environment of $\text{Sn}1$ core by its lone pair $5s^2$. b) Sn^{2+} in its fluorine equatorial plane showing the section of fluorine atoms with the detail of Fa electronic environment crowned by $\{\text{Ea}_3\}$ triplet lone pair torus. c) Section by a plane orthogonal to $\text{Sn}2$ -CT in CT showing the median plane of Ea torus domains of highest density (IDC = 0.831) indicating the pathway of the lone pair triplet on the gyration radius (yellow circle). The pale blue circle of Ea is separated by 120° in agreement with their size. d) The sequence of $\text{Sn}2$ -Fa-CT(torus)- $[\text{SnE}]1$ of the edge of the sub-cube. (For interpretation of the references to color in this figure legend, the reader is referred to the Web version of this article.)

relevant to bonding, antibonding and non-bonding interactions respectively. Clearly, the two Sn valences present different Sn-F interaction results. The main part of the VB is of bonding character (positive intensity COOP) with an energy shift leading to lower energy $\text{Sn}^{\text{IV}}\text{-F}$ (more ionic) versus $\text{Sn}^{\text{II}}\text{-F}$ (less ionic), the latter characterized by an antibonding red line in the CB designating the $5s^2$ lone pair LP character.

Therefore we can propose that the electronic structure results (DOS and COOP) together with those pertaining to stereochemistry and LP metrics present altogether a rationale of tin fluoride compounds within a holistic view.

6. Concluding notes

The aim of the present work on tin fluorides was to provide further illustration of $\text{Sn } 5s^2$ LP spatial extension and metrics within single and mixed-valence fluorides. At the same time the important role of fluorine ligand was precisely depicted, particularly when terminating a covalent bond with its lone pair triplet designing an electronic torus, which center is repulsed after F center of Sn-F bond (case of Sn-F2 bond, of $\text{SnF}_4\{\text{E}_3\}_2$) but also in $\text{Sn}_2\text{EF}_6\{\text{E}_3\}_6$ or $[\text{Sn}1\text{E}]^{2+}\text{Sn}^{4+}[\text{F}\{\text{E}_3\}]_6$.

- The Sn-E average distance appears around $0.98 \pm 0.05 \text{ \AA}$ for both

SnF_4E (TBP) or SnF_5E (O) but for $\alpha \text{SnF}_4\text{E}$ TBP this distance is more compelled by the network the value being $\text{Sn}1\text{-E}1 = 0.862 \text{ \AA}$. Therefore E-F distances equal $2.75 \pm 0.05 \text{ \AA}$ in all cases.

- $\text{Sn}_2\text{F}_6\text{E}$ has given the opportunity to evaluate the size $[\text{SnE}]1^{2+}$ cation in its fluorine octahedron which is $R = 0.93 \text{ \AA}$.

Another important result deals with the lone pair triplet $\{\text{E}_3\}$ brought by fluorine atoms as emphasized in the previous papers [3–5]. Therefore another characteristic is provided here by comparing SnF_4 (or $\text{Sn}^{4+}\text{F}_1_2[\text{F}_2\{\text{E}_3\}]_2$) and Sn_2F_6 (or $[\text{SnE}]1^{2+}\text{Sn}^{4+}\text{F}_6\{\text{E}_3\}_6$) fluorides. The $\{\text{E}_3\}$ triplet around F plays a dynamic role according to network opportunities. In $\text{SnF}_4\{\text{E}_3\}$ triplet a torus centered in CT on Sn-F2 bond axis is facing an empty space (Fig. 2) allowing a $\text{F}2\text{-CT} = 0.168 \text{ \AA}$ or $\text{Sn-CT} = \text{Sn-F}2 + 0.168 \text{ \AA} = 2.042 \text{ \AA}$; this $\{\text{E}_3\}$ torus displacement has been attributed to repulsive effect of covalent bond Sn-F2. In Sn_2F_6 , Fa is sandwiched by $[\text{Sn}1\text{E}]^{2+}$ and Sn^{2+} , so $\text{Sn}2\text{-CT} = \text{Sn}2\text{-Fa} + 0.129 \text{ \AA} = 1.993 \text{ \AA}$ showing that $[\text{SnE}]1^{2+}$ with its large size maintains an attractive force on $\{\text{E}_3\}$ torus and correlatively weakens $\text{Sn}2\text{-Fa}$ bonding repulsive effect. This situation shows that in various networks $\{\text{E}_3\}$ F torus can play an adjustment role in network architecture building.

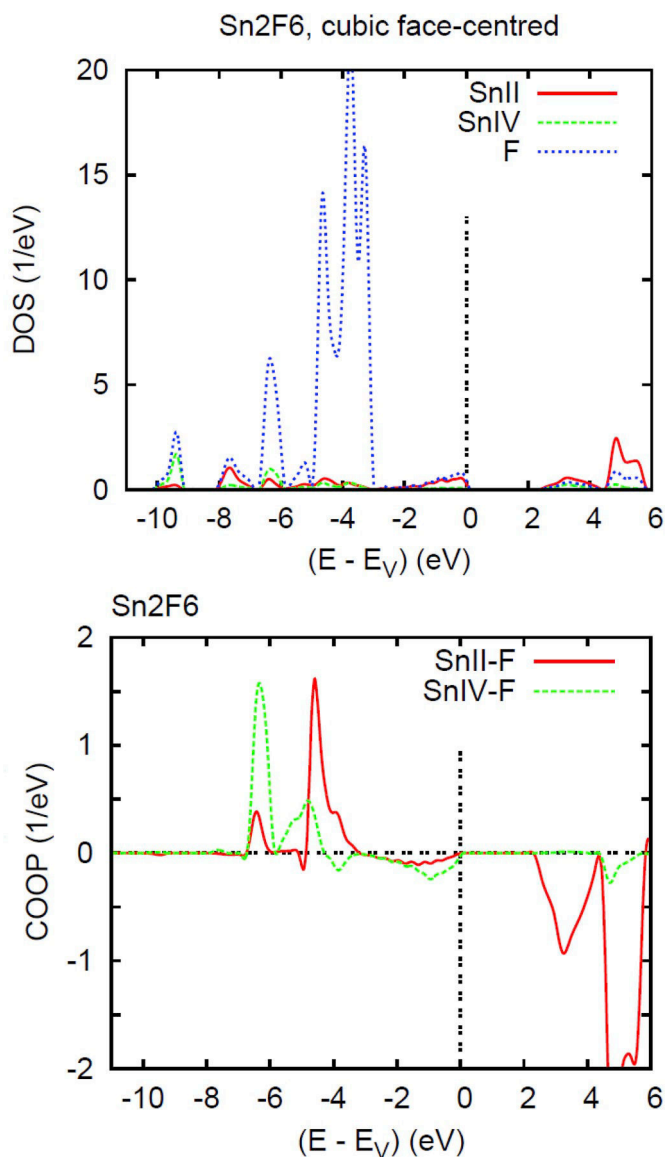


Fig. 18. Sn_2F_6 : Site projected DOS (top) and differentiated Sn(II)-F/Sn(IV)-F chemical bonding based on overlap integral S_{ij} COOP criterion (bottom).

Acknowledgments

One of us (JG) thanks LCTS-CNRS for providing laboratory facilities and G. Couégnat for his efficient support in calculations. Computational facilities provided by LGU on workstations running Linux-Suse13 OS are acknowledged.

References

- [1] Greenwood NN, Earnshaw A. second ed. Chemistry of the elements vol. 381. Oxford: Butterworth-Heinemann0-7506-3365-4; 1997.
- [2] Holleman AF, Wiberg E, Wiberg N. Inorganic chemistry. first ed. Academic Press0-12-352651-5; 2001. p. 908.
- [3] Matar SF, Galy J. Solid State Sci 2016;52:29.
- [4] Matar S, Réau J-M, Demazeau G, Lucat C, Portier J, Hagenmuller P. Solid State Commun 1980;35:681.
- [5] Matar SF, Galy J. Prog Solid State Chem 2015;43:82-97.
- [6] Dove MFA, King R, King TJ. J Chem Soc, Chem Commun 1973:944-5.
- [7] Ruchaud N, Mirambet C, Fournès L. J. Grannec. Z Anorg Allg Chem 1990;590:173.
- [8] Hohenberg P, Kohn W. Phys Rev B 1964;136:864.
- [9] Kohn W, Sham LJ. Phys Rev A 1965;140:1133.
- [10] Becke AD, Edgecombe KE. J Chem Phys 1990;92:5397.
- [11] Denes G, Pannetier J, Lucas J, Le Marouille JY. J Solid State Chem 1979;30:335.
- [12] Denes G, Pannetier J, Lucas J. J Solid State Chem 1980;33:1.
- [13] Kresse G, Furthmüller J. Phys Rev B 1996;54:11169.
- [14] Kresse G, Joubert J. Phys Rev B 1999;59:1758.
- [15] Blöchl PE. Phys Rev B 1994;50:17953.
- [16] Perdew J, Burke K, Ernzerhof M. Phys Rev Lett 1996;77:3865.
- [17] Savin A, Jepsen O, Flad J, Andersen OK, Preuss H, von Schnering HG. Angew Chem Int Ed Engl 1992;31:187.
- [18] Mostofi AA, Yates JR, Pizzi G, Lee YS, Souza I, Vanderbilt D, Marzari N. Comput. Phys. Commun. 2014;185:2309.
- [19] Houari A, Matar SF, Eyert V. Electron Struct. 2019;1:015002.
- [20] Matar SF, Houari A, Eyert V. J Magn Magn Mater 2019;491:165555.
- [21] Hoffmann R. Angew Chem Int Ed Engl 1987;26:846.
- [22] Bork M, Hoppe R. Z Anorg Allg Chem 1996;622:1557.
- [23] Galy J, Matar SF. Solid State Sci 2017;64:114.
- [24] Galy J, Couégnat G, Vila E, Matar SF. Compt Rendus Chem 2017;20:446.
- [25] Chang JH, Koehler J. Z Krist 1999;214:147.